Matting and Depth Recovery of Thin Structures using a Focal Stack Supplementary Material

Chao Liu
chaoliu1@cs.cmu.edu

Artur W. Dubrawski
awd@cs.cmu.edu

Srinivasa G. Narasimhan
srinivas@cs.cmu.edu

1. Calibrating Blur Kernel

In this section, we describe our method to calibrate the blur kernels for the light field refocused images. The optical blur kernel is assumed to be a separable filter kernel such that it can be written as a convolution of two 1D functions. In this case, the blurred image I can be written as:

$$I = L * B(x, y) = L * f(x) * f(y), \tag{1}$$

with $B(x, y) = f(x) * f(y)$ because the blur kernel is separable. To estimate the 1D blur kernels $f(x)$ and $f(y)$, we use unidirectional binary patterns as described in [2]. In our experiment, we use vertical and horizontal strip binary patterns.

For a vertical pattern as shown in Figure 1, if the blur kernel is separable, the blurred image is only related to the blur kernel in the direction of x-axis:

$$I = L * f(x) \tag{2}$$

Then we can write this 1D-convolution into a matrix form:

$$\mathbf{m} = A_x \mathbf{b}_x, \tag{3}$$

where column vector $\mathbf{m}$ is the vectorized blurred image; the column vector $\mathbf{b}_x$ is the 1D blur kernel in the x-direction; each row of the matrix A_x is the un-blurred sharp image intensities in the surrounding range in x-direction for the corresponding pixel in $\mathbf{m}$.

During calibration, given the sharp image A_x and blurred image $\mathbf{b}_x$, the 1D blur kernel $\mathbf{b}_x$ is determined by:

$$\begin{aligned} \min_{\mathbf{b}_x} \quad & \|A_x \mathbf{b}_x - \mathbf{m}\|_2 + \lambda \|\nabla \mathbf{b}_x\|_1 \\ \text{subject to} \quad & \mathbf{b}_x \succeq 0, \end{aligned} \tag{4}$$

with the second term in the energy function regularizing the shape of the blurring kernel. The optimization problem in Eq. 4 is convex and can be solved by a convex optimization solver. We use the *CVX* toolbox [1] in the implementation. The 1D blur kernel in the y-axis direction is optimized in the same way using a vertical binary pattern.

With the estimated 1D blur kernels $f(x)$ and $f(y)$, the blur kernel $B(x, y)$ can be determined as:

$$B(x, y) = f(x) * f(y). \tag{5}$$

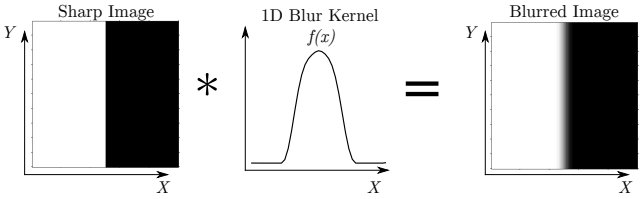

Figure 1: The optical blur for a vertical binary edge pattern. The blur kernel is assumed to be separable, so the blurred image of the vertical pattern is independent from the blur kernel in the y-axis $f(y)$.

We repeat the above calibration with 26 focal settings for a set of 21 reference depths from 200 mm to 1000 mm equally spaced with 40 mm. The calibrated blur kernels of refocused image for a plane placed 680 mm from the light field camera are shown in Figure 2. Note that the shape of the blur kernel is not circularly symmetrical since the blur kernel for a refocused image from light field camera is related to both the main lens shape and the arrangement of the secondary lenslets array.

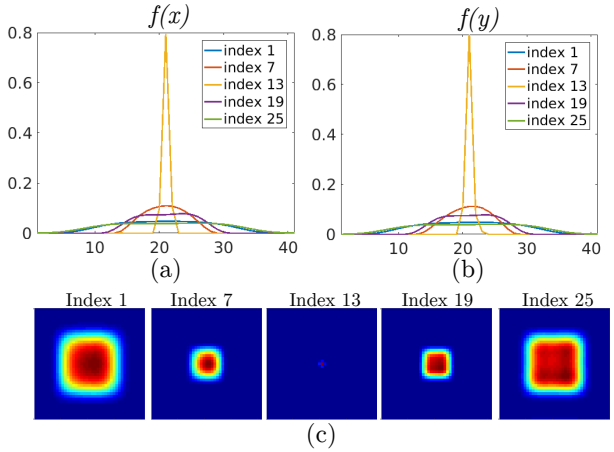

Figure 2: The calibrated blur kernels of refocused image for a plane placed 680 mm from the light field camera. (a)(b)The 1D blur kernels $f(x)$ and $f(y)$. (c)The blur kernels. The shapes of the blur kernels are not circularly symmetrical since the blur kernel for a refocused image from light field camera is related to both the main lens shape and the spatial arrangement of the secondary lenslets.

To get the differential blur kernel $\frac{\partial B}{\partial d}$ used in Section 5

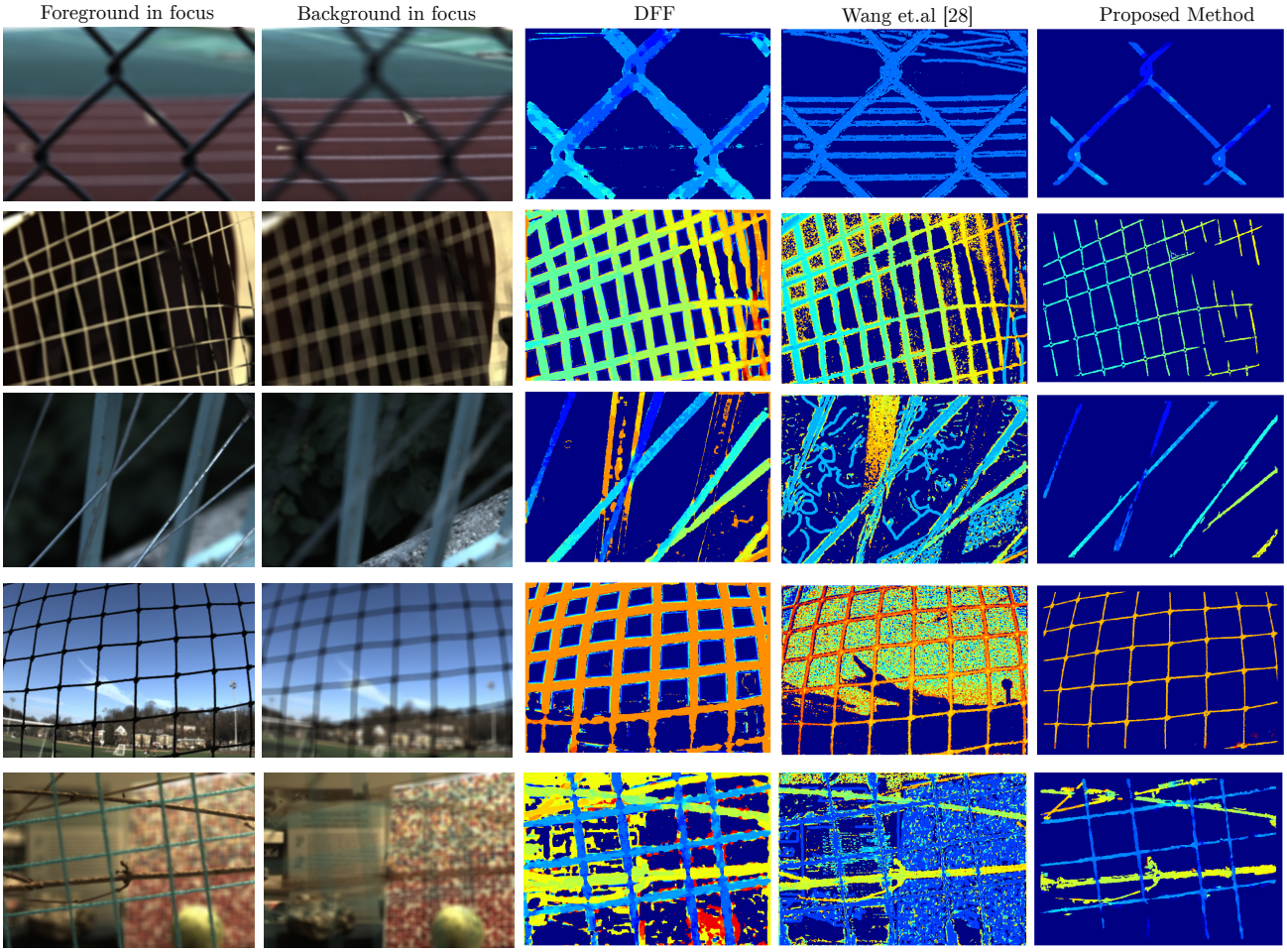

Figure 3: The depth recovery for the thin structures. Note that the depth estimations using the DFF method for points close to the occlusion boundaries are inaccurate due to high frequency depth discontinuity. The light field method indoes not perform well on the textureless regions and sharp edges in the background. Our method recovers the sharp depth discontinuity on the boundaries of the thin structures.

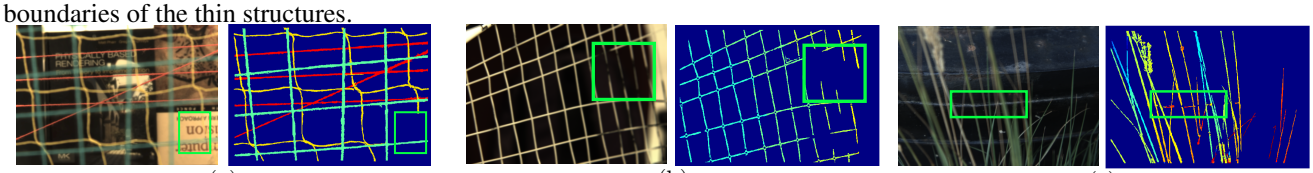

Figure 4: Limitations of our method. (a)(b) In the box marked in green, the thin structures in the near field have similar color as the background. In this case, the matting estimation fails because switching the occlusion matte values for the points in those regions will not introduce enough image intensity changes. (c) The depth of the background is close to the depth of the thin occluder, thus the estimated occlusion matte includes edges in the background.

in the paper for estimating the depth, w1e assume the blur kernel changes smoothly w.r.t. the depth. So we can approximate the differential blur kernel as:

$$\frac{\partial B}{\partial d}(d_i) \approx \frac{B(d_i + \Delta d) - B(d_i)}{\Delta d} \tag{6}$$

2. More Results

We include more comparison results in Figure 3.

3. Limitations

As explained in the paper, our methods have several limitations. First, if the thin structures in the near field have similar color as the background. the occlusion matting estimation may fail because switching the occlusion matte values for the points in those regions will not introduce enough image intensity changes, as shown in Figure 4(a)(b).

Second, when the depth of the background is close to the depth of the thin occluder, the occlusion matte estimation tends to include the edges in the background as thin structures/occlusion boundaries, as shown in Figure 4(c).

References

[1] M. Grant and S. Boyd. CVX: Matlab software for disciplined convex programming, version 2.1. http://cvxr.com/cvx, Mar. 2014.

[2] H. Ha, Y. Bok, K. Joo, J. Jung, and I. S. Kweon. Accurate camera calibration robust to defocus using a smartphone. In *Proceedings of the 2015 IEEE International Conference on Computer Vision (ICCV)*, ICCV 15, pages 828–836, Washington, DC, USA, 2015. IEEE Computer Society.